

Three-Dimensional Structure and Reactivity of a Photochemical Cleavage Agent Bound to DNA

Susan M. Gasper, Bruce Armitage,[†] Xiuqi Shui, Gary G. Hu, Changjun Yu, Gary B. Schuster,* and Loren Dean Williams*

Contribution from the School of Chemistry & Biochemistry, Georgia Institute of Technology, Atlanta, Georgia 30332-0400

Received May 20, 1998

Abstract: Irradiation of the anthraquinone derivative *N,N*-Bis(3-aminopropyl)-2-anthraquinonesulfonamide dihydrochloride (AQS2) when bound to DNA leads to strand cleavage, primarily at GG steps. The 1.8 Å X-ray structure of AQS2 bound to the DNA duplex [d(CGTCAG)]₂ shows an intercalated, groove-reversed complex with the out-of-plane “swallow tail” located in the major groove. Two molecules of AQS2 bind with the chromophores intercalated at each CG step. Extensive guanine–AQS2 interactions are observed in the intercalated complex, indicating that the ground-state anthraquinone and DNA are poised for efficient electron transfer after photoexcitation. AQS2 engages in guanine-selective van der Waals contacts and molecular orbital overlap. Molecular orbitals, calculated using coordinates of the X-ray structure, confirm the extensive electronic overlap between the redox partners. The bases adjacent to the intercalation site are well-stacked. The structure supports a model in which electron transfer from base to AQS2 and hole migration within DNA require significant electronic overlap.

DNA in its biological environment is oxidatively damaged by the products of normal metabolic processes,¹ by ionizing radiation,^{2,3} and by light.⁴ One mechanism of these reactions involves the loss of an electron by a DNA base to form a radical cation (electron hole). Interest in such radical cations has expanded as a consequence of the discovery that their formation by electronically excited small molecules such as riboflavin,⁵ naphthalimide,⁶ rhodium complexes (Rh),⁷ and a series of anthraquinone (AQ) derivatives⁸ provides a model for natural oxidative processes.

We showed that the DNA-binding mode of AQ derivatives is controlled by their structure. Most monosubstituted cationic anthraquinones intercalate; others appear to groove-bind.⁹ The binding mode determines the mechanism of reaction.¹⁰ Irradiation of intercalatively bound anthraquinones generates base radical cations. A radical cation can migrate from base to

base along the DNA stack. Such hole migration through DNA is well-documented and well-accepted, but the rate of this process is still uncertain. Barton and co-workers have inferred an extremely rapid rate of migration;¹¹ others contend that the rate is slower.^{12–14} The discrepant results may arise from differing extents of orbital interaction among electron acceptors and DNA bases in various experimental systems. Ultimately a migrating radical cation is stopped at a trap where it reacts irreversibly. The trapped radical cation causes strand cleavage.¹⁵

Our long-term goal is to determine how three-dimensional structures of DNA and DNA complexes direct efficiency and mechanism of photocleavage, initiating with photoexcitation, then DNA base to chromophore electron transfer, hole migration, trapping, and covalent oxidative damage. Here we describe the three-dimensional structure of the anthraquinone AQS2 bound to a DNA fragment determined by X-ray crystallography. The X-ray structure can help relate intercalation, extent of base–intercalator interaction, and base–base stacking to efficiency of electron transfer. AQS2 intercalates in DNA, interacting extensively with the DNA bases. Extensive overlap of molecular orbitals in the intercalated AQS2 complex helps explain the very rapid transfer of an electron to the excited quinone from its flanking DNA bases. The DNA bases adjacent to the intercalation site remain stacked, providing an efficient route for base to base hole migration. These results allow us to link the structure of the intercalated anthraquinone to the reaction of the DNA caused by its irradiation.

[†] Current address: Department of Chemistry, Carnegie Mellon University, 4400 Fifth Ave., Pittsburgh, PA 15213.

(1) Cheng, K. C.; Cahill, D. S.; Kasai, H.; Nishimura, S.; Loeb, L. A. *J. Biol. Chem.* **1992**, *267*, 166–172.

(2) Boon, P. J.; Cullis, P. M.; Symons, M. C. R.; Wren, B. W. *J. Chem. Soc., Perkin Trans. 2* **1984**, 1393–1399.

(3) Wolf, P. G.; Jones, D. D.; Candeias, L. P.; O'Neill, P. *Int. J. Radiat. Biol.* **1993**, *64*, 7–18.

(4) Melvin, T.; Plumb, M. A.; Botchway, S. W.; O'Neill, P.; Parker, A. W. *Photochem. Photobiol.* **1995**, *61*, 584–591.

(5) Kasai, H.; Yamaizumi, Z.; Berger, M.; Cadet, J. *J. Am. Chem. Soc.* **1992**, *114*, 9692–9694.

(6) Matsugo, S.; Kawanishi, S.; Yamamoto, K.; Sugiyama, H.; Matsuura, T.; Saito, I. *Angew. Chem., Int. Ed. Engl.* **1991**, *30*, 1351–1353.

(7) Arkin, M. R.; Stemp, E. D.; Pulver, S. C.; Barton, J. K. *Chem. Biol.* **1997**, *4*, 389–400.

(8) Ly, D.; Kan, Y.; Armitage, B.; Schuster, G. B. *J. Am. Chem. Soc.* **1996**, *118*, 8747–8748.

(9) Breslin, D. T.; Yu, C.; Ly, D.; Schuster, G. B. *Biochemistry* **1997**, *36*, 10463–10473.

(10) Breslin, D. T.; Coury, J. E.; Anderson, J. R.; McFail-Isom, L.; Kan, Y.; Williams, L. D.; Bottomley, L. A.; Schuster, G. B. *J. Am. Chem. Soc.* **1997**, *119*, 5043–5044.

(11) Arkin, M. R.; Stemp, E. D. A.; Holmlin, R. E.; Barton, J. K.; Horman, A.; Olson, E. J. C.; Barbara, P. F. *Science* **1996**, *273*, 475–480.

(12) Lincoln, P.; Tuite, E.; Norden, B. *J. Am. Chem. Soc.* **1997**, *119*, 1454–1455.

(13) Pratt, F.; Hou, C.-C.; Foote, C. S. *J. Am. Chem. Soc.* **1997**, *119*, 5051–5052.

(14) Takana, K.; Fukui, K. *Angew. Chem., Int. Ed. Engl.* **1998**, *37*, 158.

(15) Gasper, S. M.; Schuster, G. B. *J. Am. Chem. Soc.* **1997**, *119*, 12762–12771.

Methods

Synthesis. 2-Antraquinonesulfonic acid was purchased from Aldrich. 2-Antraquinonesulfonyl chloride¹⁶ and bis[3-[(1-butoxycarbonyl)amino]propyl]amine hydrochloride⁹ were synthesized as previously described. ¹H NMR spectra were obtained on a GE QE-300 (300 MHz) spectrometer. Melting points were taken on a Büchi melting point apparatus and are uncorrected. Elemental analyses were performed by the University of Illinois Microanalysis Laboratory.

***N,N*-Bis[3-[(*tert*-butoxycarbonyl)amino]propyl]-2-antraquinonesulfonamide (Boc-protected AQS2)** was prepared in 62% yield by stirring a solution of 1.5 mL of triethylamine, 0.25 g (0.68 mmol) of bis[3-[(1-butoxycarbonyl)amino]propyl]amine hydrochloride, and 0.21 g (0.67 mmol) of 2-antraquinonesulfonyl chloride in 50 mL of dichloromethane overnight. The mixture was washed twice with water, dried over anhydrous sodium sulfate, and concentrated to a volume of 3 mL, to which 100 mL of hexane was added. The precipitate was filtered off and washed once with hexane to give 0.25 g of Boc-protected AQS2: mp 154–156 °C; ¹H NMR (CDCl₃) δ 1.43 (s, 18 H), 1.76 (q, *J* = 6.6 Hz, 4 H), 3.16–3.27 (m, 8 H), 4.89 (br s, 2 H), 7.85–7.88 (m, 2 H), 8.20 (dd, *J* = 8.1 Hz, 1.5 Hz, 1 H), 8.33–8.37 (m, 2 H), 8.46 (d, *J* = 8.1 Hz, 1 H), 8.69 (d, *J* = 1.5 Hz, 1 H). Anal. Calcd for C₃₀H₃₉N₃SO₄: C, 59.89; H, 6.53; N, 6.98. Found: C, 59.70; H, 6.63; N, 6.98.

***N,N*-Bis(3-aminopropyl)-2-antraquinonesulfonamide dihydrochloride (AQS2)** was prepared in 87% yield by the addition of 10 mL of a 1 N HCl–ether solution to a solution of 0.11 g (0.18 mmol) of *N,N*-bis[3-[(*tert*-butoxycarbonyl)amino]propyl]-2-antraquinonesulfonamide in 20 mL of methanol and 10 mL of dichloromethane. The mixture was stirred for 5 h, after which it was concentrated to 3 mL, followed by the addition of 120 mL of diethyl ether. The precipitate was filtered off and washed once with ether to give 0.08 g of AQS2: mp 250 °C dec; ¹H NMR (D₂O) δ 1.96 (q, *J* = 6.9 Hz, 4 H), 2.55 (t, *J* = 6.9 Hz, 4 H), 3.36 (t, *J* = 6.9 Hz, 4 H), 4.80 (br s, 6 H), 7.81–7.84 (m, 2 H), 8.00–8.05 (m, 2 H), 8.17 (s, 2 H), 8.32 (s, 1 H); ¹³C NMR (D₂O spiked with CH₃OH as a reference) δ 38.7, 49.0 (CH₃-OH), 56.8, 58.5, 61.0, 137.2, 139.2, 140.8, 143.8, 143.9, 144.4, 145.1, 147.0, 147.7, 147.8, 155.0, 194.0, 194.1. Anal. Calcd for C₂₀H₂₅N₃SO₄·2H₂O: C, 48.79; H, 5.53; N, 8.53. Found: C, 48.96; H, 5.47; N, 8.79.

Cleavage Analysis by Radiolabeling and PAGE. The 25-mer oligonucleotide was radiolabeled at the 5'-OH using [^γ-³²P]ATP and bacterial T4 polynucleotide kinase.¹⁷ Radiolabeled DNA was purified by 20% PAGE. Samples for irradiation were prepared by hybridizing a mixture of cold and radiolabeled oligonucleotide (5 μM) with 5 μM of the complementary strand and 20 μM AQS2 in 10 mM phosphate buffer, pH 7. Hybridization was achieved by heating the samples at 80 °C for 5 min and slowly cooling to room temperature. These samples were irradiated in microcentrifuge tubes in a Rayonet photo-reactor containing eight 350 nm lamps. After irradiation, the samples were precipitated and then treated with hot piperidine for 30 min. Samples (1000 cpm) were separated by electrophoresis on 20% denaturing 19:1 acrylamide–bis(acrylamide) gel containing 7 M urea. Gels were dried, and the cleavage was visualized by autoradiography.

Phosphorescence Quenching. Solutions of 20 μM AQS2 in 2:1 (v/v) 10 mM pH 7 phosphate buffer–ethylene glycol were prepared and transferred to NMR tubes, which were then submerged in an optical Dewar flask containing liquid nitrogen. The samples were excited at 334 nm, and the phosphorescence emission spectra were recorded from 400 to 600 nm. Samples containing AQS2 and DNA were prepared as described above and contained 200 μM calf thymus DNA (base pairs) in addition to 20 μM AQS2.

Crystallization. The ammonium salt of reverse-phase HPLC purified d(CGTACG) was purchased from the Midland Certified Reagent Co. (Midland, TX). Crystals were grown at room temperature from sitting drops that initially contained 1.8 mM d(CGTACG), 21 mM sodium cacodylate (pH 6.5), 3.3 mM MgCl₂, 1.1% 2-methyl-2,4-

Table 1. Data Collection and Refinement Statistics for the Complex of CGTACG with AQS2

space group	P6 ₅ 22
unit cell <i>a</i> (Å)	31.02
unit cell <i>c</i> (Å)	64.91
temp of data collcn (°C)	−137
<i>R</i> -merge (%) ^a	7.7
<i>R</i> -factor (%)	19.6
<i>R</i> -free (%)	26.8
no. of reflns collected	24 530
no. of unique reflns (1.8–10 Å)	1972
no. of reflns used for refinement (includes test set)	1680 ^b
rms dev of bonds from ideality (Å)	0.014
rms dev of angles from ideality (deg)	3.025
statistics for highest resolution shell (1.80–1.88 Å)	145 reflns 30.2 <i>R</i> -factor 65.6% completeness

^a *R*-merge = sum(abs(ave − obs))/sum(ave). ^b For data with *F* > 5σ(*F*). ^c For the working set, after sequestering 10% for *R*-free.

pentanediol (MPD), 0.8 mM spermine trihydrochloride, and 1.5 mM AQS2. Crystallization droplets were equilibrated by vapor diffusion against a reservoir of 10% MPD. Hexagonal crystals appeared within 1 month. These crystals stopped growing while too small for data collection and so were transferred to 10 μL droplets under initial crystallization conditions. Crystal growth was reinitiated and progressed over 20–40 days. A well-formed crystal of dimensions 0.15 × 0.25 × 0.15 mm³ was plucked up in a loop and transferred directly into a −137 °C N₂ stream bathing the goniostat.

Data Collection and Reduction. X-ray intensity data were collected at low temperature (−137 °C) with multiwire detectors (ADSC). Copper Kα radiation (λ = 1.542 Å) was generated with a fine-focus Rigaku RU200 rotating anode and monochromated with a graphite grating. Data were merged and reduced with ADSC software. Space group, unit cell parameters, and data collection and reduction statistics are given in Table 1.

Structure Solution and Refinement. This structure was solved by molecular replacement using a portion of the structure of D232–[d(CGTACG)]₂ as the initial model. D232 is a bis-intercalator.¹⁸ The structure of a D232–dCGTACG complex was solved by MAD phasing (X.S. and L.D.W., unpublished). The unit cell of the D232–dCGTACG complex (28, 28, 74 Å, space group *P*6₅22) is roughly similar to that of the AQS2–d(CGTACG) complex. The initial AQS2–DNA model 1/2((D232–[d(CGTACG)]₂) minus the linker) was transformed to the AQS2–d(CGTACG) unit cell and was refined as a rigid body. The model was modified by switching the chromophore from that of D232 to that of AQS2. This model was refined by segmented rigid-body refinement and then by simulated annealing and positional refinement with XPLOR (version 3.1)¹⁹ using the parameter file dna-rna-multi-endo.param.^{20,21} At that point sum (2*F*_o − *F*_c) and difference (*F*_o − *F*_c) Fourier maps clearly revealed the swallow tail of AQS2 within the major groove. The model had not previously incorporated any structural features similar to the swallow tail. The observation of clear density for the swallow tail was taken as definitive evidence that the solution was correct. The swallow tail was docked into density, and the model was treated with both positional and thermal factor refinement. Water molecules were added to corresponding sum and difference peaks. Models were displayed and manipulated on a graphics terminal with the program CHAIN.²² Helical parameters were calculated with the program CURVES.²³

(18) Garbay-Jaureguiberry, C.; Laugaa, P.; Delepierre, M.; Laalami, S.; Muzard, G.; Le Pecq, J. B.; Roques, B. P. *Anti-Cancer Drug Des.* **1987**, *1*, 323–335.

(19) Brunger, A. *XPLOR*, version 3.1; The Howard Hughes Medical Institute, Yale University: New Haven, CT, 1992.

(20) Clowney, L.; Jain, S. C.; Srinivasan, A. R.; Westbrook, J.; Olson, W. K.; Berman, H. M. *J. Am. Chem. Soc.* **1996**, *118*, 509–518.

(21) Gelbin, A.; Schneider, B.; Clowney, L.; Hsieh, S.-H.; Olson, W. K.; Berman, H. M. *J. Am. Chem. Soc.* **1996**, *118*, 519–529.

(16) Armitage, B. A.; Yu, C.; Devadoss, C.; Schuster, G. B. *J. Am. Chem. Soc.* **1994**, *116*, 9847–9859.

(17) Sambrook, J.; Fritsch, E. F.; Maniatis, T. *Molecular Cloning. A Laboratory Manual*; Cold Spring Harbor Press: Cold Spring Harbor, NY, 1989.

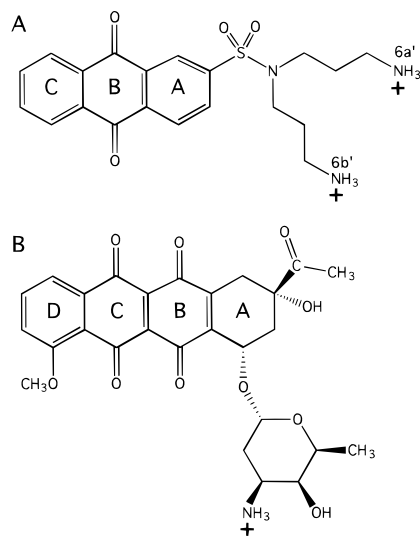


Figure 1. Chemical structures of (A) the dicationic anthraquinone AQS2 and (B) the anthracycline daunomycin.

Results

Solution Binding. AQS2 is an anthraquinone substituted at the 2-position with a sulfonamide-linked dication (Figure 1A). The dicationic out-of-plane substituent on the planar quinone chromophore is referred to here as a “swallow tail” because of the shape of its sulfonamide and two alkylammonium groups. Spectral analyses of anthraquinone derivatives reveals the strength and mode of their association with DNA. The equilibrium constant for binding of AQS2 to calf thymus DNA, determined from a competitive ethidium bromide displacement assay,¹⁶ is $2.0 \times 10^5 \text{ M}^{-1}$ in a solution containing 10 mM sodium phosphate and 100 mM sodium chloride at pH 7.0.

Analysis of the UV absorbance spectrum and phosphorescence quenching data for AQS2 suggests that it binds to duplex DNA by intercalation. In the presence of calf thymus DNA, the absorption band of free AQS2, which is centered at 335 nm, undergoes a slight red shift and exhibits a 36% hypochromicity (Figure 2). These spectral changes are similar to those for anthraquinones known to intercalate.

Anthraquinones phosphoresce strongly in frozen solution. In the absence of DNA, excitation of AQS2 in a glassy matrix at 77 K gives strong phosphorescence from its $n\pi^*$ triplet state (Figure 2). When this quinone is bound to calf thymus DNA, the phosphorescence is completely quenched. Phosphorescence quenching is attributed to rapid electron transfer from a DNA base to the excited triplet state of the quinone. This result confirms that AQS2 intercalates in duplex DNA since groove binding does not provide the π -electron overlap required for complete phosphorescence quenching.

Photocleavage of DNA by AQS2. Irradiation of anthraquinone derivatives substituted with electron-withdrawing amide groups related to AQS2 leads to damage selectively at the 5'-G of GG steps of duplex DNA. We examined the photochemistry of AQS2 with DNA to see if it follows this pattern.

A 25-base-pair DNA duplex containing several GG sites was used as a substrate to determine sites of photocleavage by AQS2 (Figure 3). Irradiation of the bound complex (350 nm) and separation of reaction products by gel electrophoresis reveal preferential cleavage, after piperidine treatment, at 5'-GG-3'

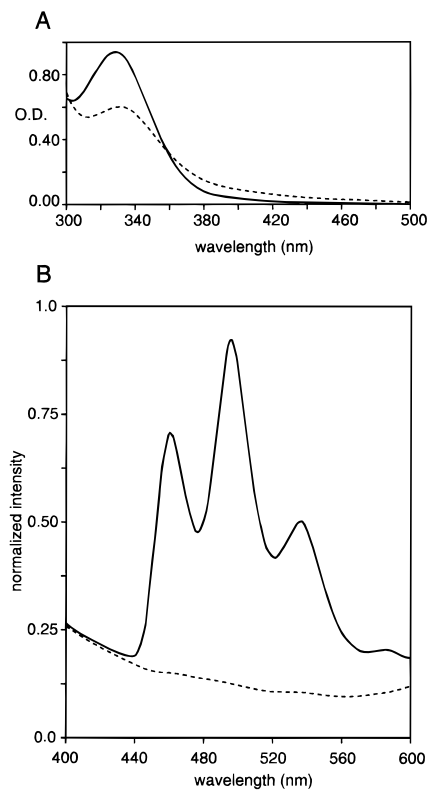


Figure 2. (A) Absorbance spectra of AQS2 alone (solid) and in the presence of calf thymus DNA (dashed). (B) Phosphorescence spectra of AQS2 alone (solid) and in the presence of calf thymus DNA (dashed) at 77 K in phosphate buffer and 33% (v/v) ethylene glycol.

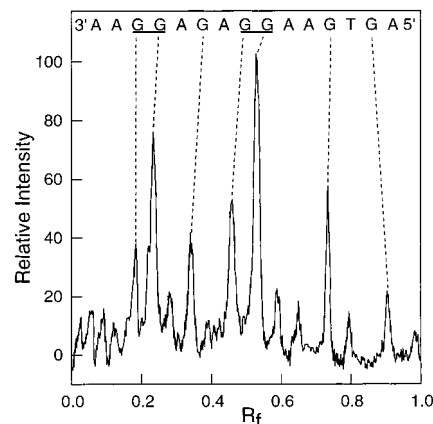


Figure 3. Histogram of the light-induced cleavage reaction after irradiation of a DNA 25-mer plus AQS2. Preferential cleavage at the 5'-G of GG doublets, underlined, is apparent.

steps, with the greater cleavage at the 5'-G. This is the same pattern of reactivity seen for many of the other monosubstituted anthraquinone derivatives we have examined.

Three-Dimensional Structure of An AQS2–DNA Complex. The solution experiments with AQS2 and related anthraquinones suggest that they bind to DNA by intercalation. We reconfirm this conclusion by X-ray crystallography, which has allowed us to visualize the intercalated complex on a molecular level.

The 1.7 Å resolution structure demonstrates that AQS2 intercalates in the DNA hexamer duplex $[\text{d}(\text{CGTACG})_2]$. The electron density maps are clean and continuous around both DNA and AQS2 (Figure 4). The DNA residues are labeled 5' C(1), G(2), T(3), A(4), C(5), G(6) 3' for the first strand and 5' C(7), G(8), T(9), A(10), C(11), G(12) 3' for the second strand

(22) Sack, J. *Chain: A Crystallographic Modelling Program*; Baylor College of Medicine: Waco, TX, 1990.

(23) Lavery, R.; Sklenar, H. *J. Biomol. Struct. Dynam.* **1989**, *6*, 655–667.

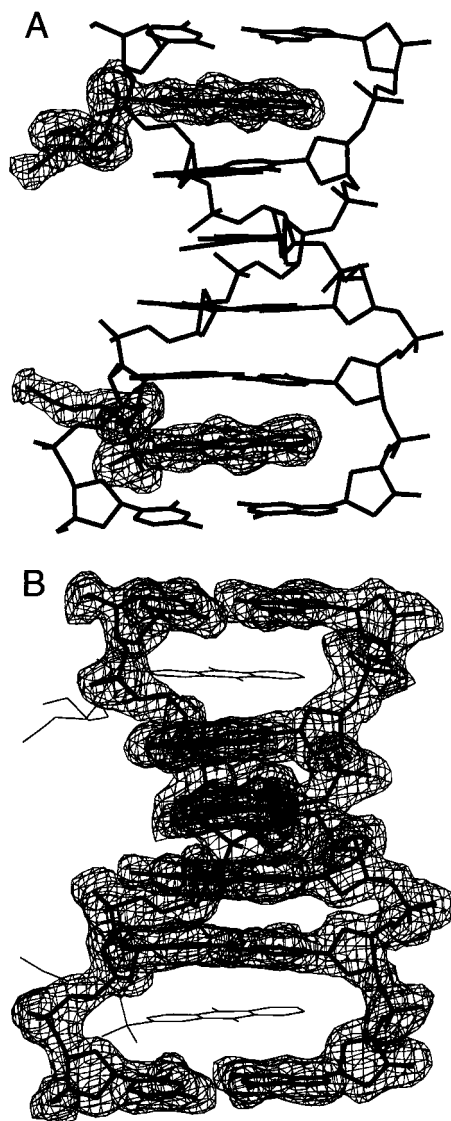


Figure 4. Sum Fourier density maps ($2F_o - F_c$) contoured at 1σ surrounding (A) AQS2 and (B) the DNA hexamer duplex.

(Figure 5). Base pairs are C(1)–G(12), G(2)–C(11), and so on. AQS2 intercalates between base pairs C(1)–G(12) and G(2)–C(11) and between base pairs C(5)–G(8) and G(6)–C(7) (Table 2). The asymmetric unit consists of a single strand of DNA and one AQS2 molecule. A crystallographic 2-fold rotation axis passes between the T(3)–A(10) and A(4)–T(9) base pairs, such that C(1) is crystallographically identical to C(7), etc.

AQS2 forms a groove-reversed complex, with the swallow tail located in the major groove (Figures 5 and 6) rather than in the minor groove. This aspect of the complex was a surprise; intercalative complexes are most commonly characterized by interactions within the minor groove. Placement of the swallow tail in the major groove results from a rotation of AQS2 by 105° around the DNA helical axis, in comparison to intercalated daunomycin (Figures 5 and 6). The swallow tail does not make direct contacts with the major groove of DNA duplex into which it is intercalated. This lack of interaction may arise from lattice interactions. The swallow tail interacts with symmetry-related complexes (Table 3). One of the carbonyl oxygen atoms forms a hydrogen bond with the N4 of an adjacent cytosine. Both the terminal amino groups engage in hydrogen bonds to phosphate groups.

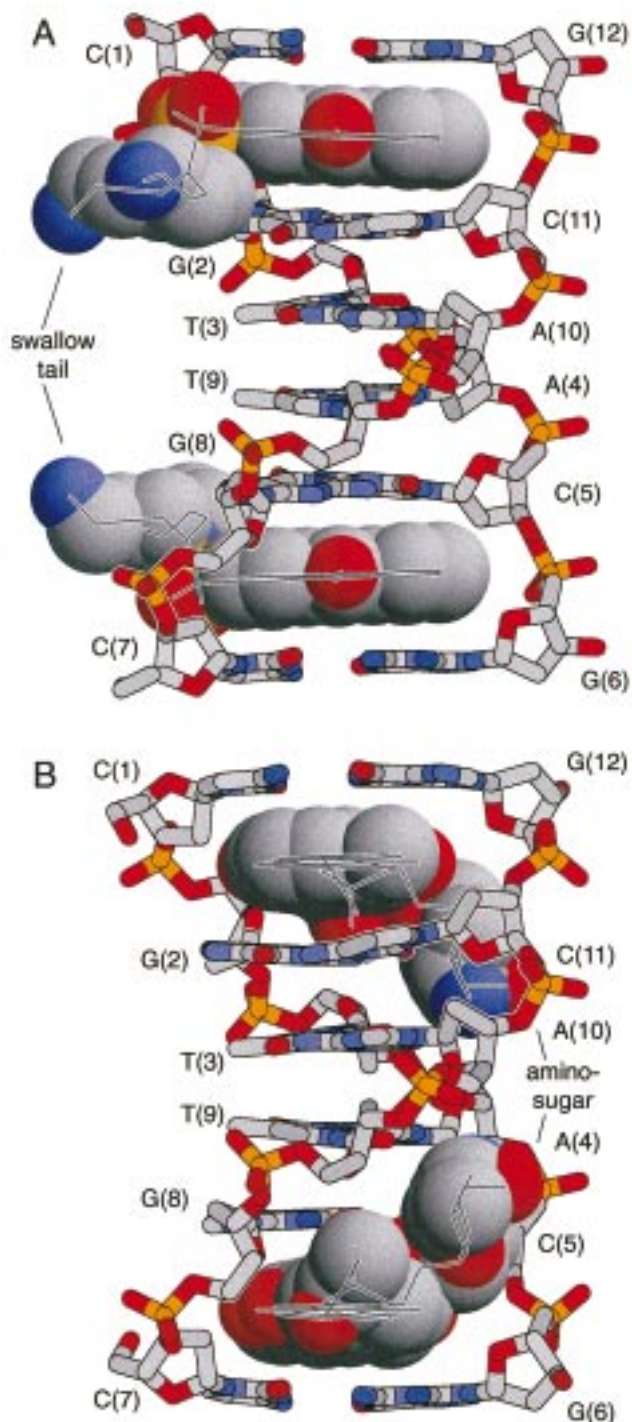


Figure 5. (A) The AQS2–d(CGATACG) hexamer duplex and (B) the daunomycin–d(CGATACG) hexamer duplex. The DNA is represented in stick form, and the drug is represented in space-filling form. Atoms are colored according to the CPK standard.

The planar aromatic surfaces of AQS2 stack preferentially with the guanine bases. The planar portion of intercalated AQS2 is flanked by two guanine bases and two cytosine bases. Five base atoms of G(12) and eight atoms of G(2) are within 3.5 \AA of the chromophore of AQS2. Only two atoms of C(1) and one atom of C(11) are within this distance of the AQS2 chromophore. This preference of AQS2 for guanines over cytosines is apparent in the axial views of Figure 6A,B. The B and C rings of AQS2 are positioned predominantly under the base of G(12) (Figure 6A). The A and B rings are positioned

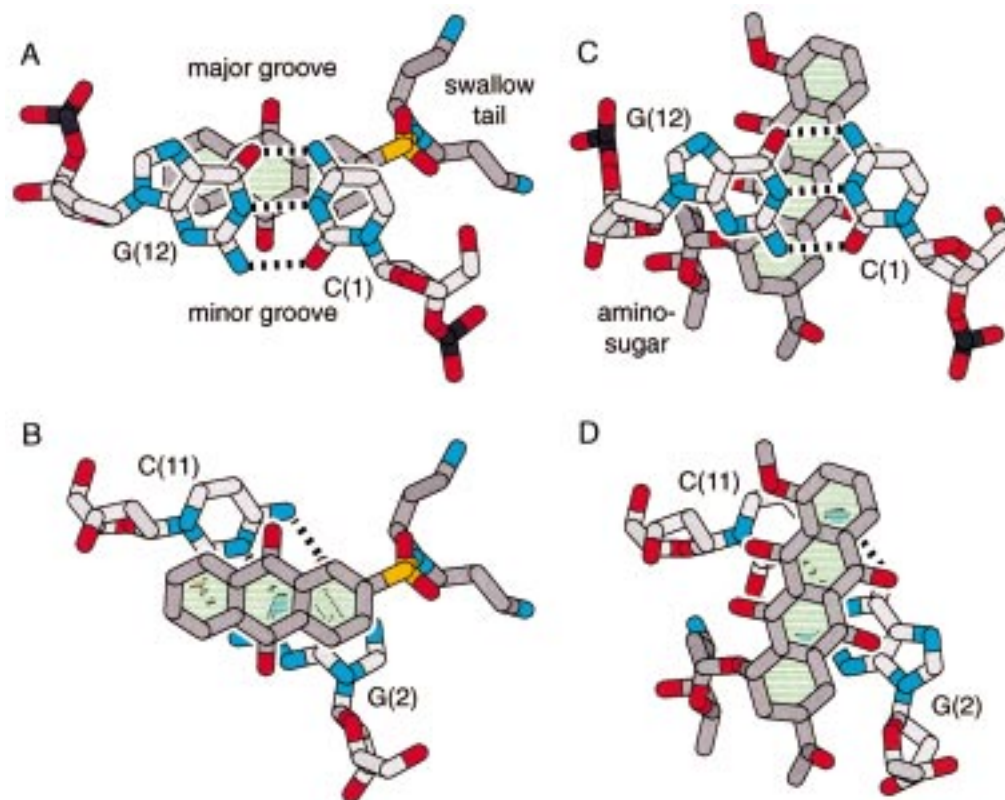


Figure 6. Axial views of intercalated DNA: (A) the C(1)–G(12) base pair over AQS2; (B) AQS2 over G(2)–C(11); (C) C(1)–G(12) over daunomycin; (D) daunomycin over G(2)–C(11). Oxygen is red, nitrogen is blue, phosphorus is black, sulfur is yellow, and carbon is gray. The carbon atoms of the intercalators are darker than those of the DNA. Hydrogen bonds are indicated by dashed lines.

Table 2. Helical Parameters for AQS2-d(CGTACG)^{a,b}

Global Base–Base Parameters				
base pair	buckle (deg)	propel (deg)	opening (deg)	
C(1)–G(12)	–0.8 (–9.9)	4.8 (0.6)	–7.0 (–9.2)	
G(2)–C(11)	–17.0 (2.8)	–4.0 (–12.6)	–0.4 (–6.6)	
T(3)–A(10)	–0.2 (4.9)	–10.0 (–4.6)	–0.5 (–8.7)	
A(4)–T(9)	0.2 (–4.8)	–10.0 (–4.7)	–0.5 (–8.7)	
C(5)–G(8)	16.9 (–2.9)	–4.0 (–12.5)	–0.4 (–6.6)	
G(6)–C(7)	0.8 (9.9)	4.8 (0.6)	–7.0 (–9.2)	
Global Inter-Base Pair Parameters				
base pairs	slide (Å)	rise (Å)	roll (deg)	twist (deg)
C(1)–G(12)/G(2)–C(11)	0.4 (0.0)	7.1 (0.0)	–9.6 (–4.6)	33.0 (–3.1)
G(2)–C(11)/T(3)–A(10)	–0.2 (0.2)	2.8 (0.0)	3.4 (1.0)	27.4 (–2.2)
T(3)–A(10)/A(4)–T(9)	–0.2 (0.1)	3.4 (0.0)	9.6 (0.2)	36.8 (1.6)
A(4)–T(9)/C(5)–G(8)	–0.2 (0.2)	2.8 (0.0)	3.5 (1.1)	27.4 (–2.2)
C(5)–G(8)/G(6)–C(7)	0.4 (0.0)	7.1 (0.0)	–9.6 (–4.7)	33.0 (–3.1)

^a Calculated with the program CURVES 3.1.²³ ^b The values in parentheses are Δ helical parameters: AQS2–d(CGTACG) minus daunomycin–d(CGTACG).

Table 3. Contacts between the AQS2 Swallow Tail and DNA

AQS2 atom	DNA residue	DNA atom	dist (Å)
O(1S)	C(1) ^a	N4	2.90
N(6a')	A(4) ^b	O2P	3.35
N(6b')	A(4) ^b	O1P	2.97
N(6b')	G(6) ^c	O6	3.15

^a Related by symmetry operator ($x, x - y, 5/6 - z$). ^b ($y, y - x, 1/6 + z$). ^c ($y - x, -x, 1/3 + z$).

predominantly over the base of G(2). The base pairs on the interior of the complex are well-stacked.

In the AQS2 complex, the DNA is unwound by only a few degrees at the intercalation site. Helical parameters for the

AQS2 complex are given in Table 2. The winding angle at the intercalation site is less in the AQS2 complex than in the daunomycin complex. Differences in helical parameters of DNA–AQS2 and DNA–daunomycin are given in Table 2. The long axis of AQS2 is aligned roughly parallel with the long axis of the flanking base pairs (Figure 6A,B). Base pair G(2)–C(11) is buckled by over 15°, wrapping around the intercalator to maximize van der Waals contacts.²⁴ Base pair C(1)–G(12) is significantly less buckled in the AQS2 complex (–0.8°) than in the daunomycin complex (–9.1°).

(24) Williams, L. D.; Egli, M.; Gao, Q.; Rich, A. *Structure & Function, Volume 1: Nucleic Acids*; Sarma, R. H., Sarma, M. H., Eds.; Adenine Press: Albany, N.Y., 1992; pp 107–125.

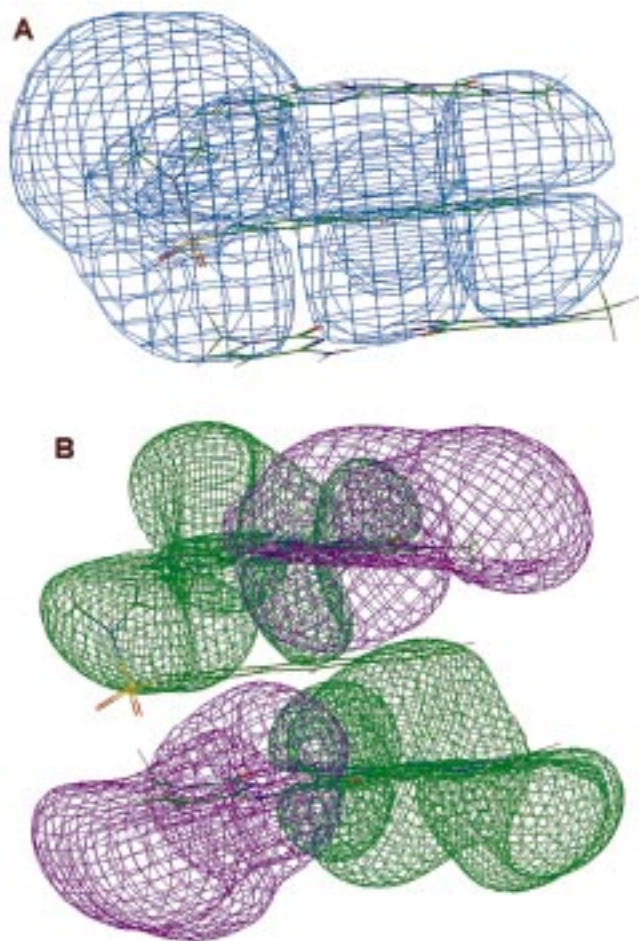


Figure 7. Molecular orbitals of AQS2 plus the two flanking base pairs. Density is contoured at approximately 95% probability: (A) LUMO for AQS2; (B) HOMO for the flanking DNA base pairs.

In parallel orientation as observed for AQS2, the flanking base pair is flattened by the chromophore; van der Waals interactions are maximized by maintaining planarity of the base pair.²⁴

In a complex with a DNA hexamer, one must be concerned about end effects. In the complex described here, AQS2 binds to the hexamer duplex at the terminal intercalation sites. It is conceivable that the structure of the complex would be different at an internal site of a long DNA fragment.

Molecular Orbital Overlap. The AQS2 LUMOs and the base HOMOs are the molecular orbitals involved in the DNA base to AQS2 electron-transfer reaction. Calculations show that these molecular orbitals overlap in the intercalated complex. The appropriate orbitals are shown in Figure 7. For simplicity, AQS2 was converted to its *N,N*-dimethylsulfonamide and the deoxyribose sugars of the flanking nucleotides were replaced with methyl groups. LUMOs for AQS2 and the HOMOs for the bases were calculated with the CVFF force field and AM1 Hamiltonian on a Silicon Graphics Indigo using InsightII.

Discussion

AQS2 binds to duplex DNA by intercalation and selectively cleaves DNA at GG dinucleotide steps. The G on the 5' side of the doublet is generally cleaved preferentially over the G on the 3' side. We have shown that this selectivity is observed for other anthraquinone derivatives with AQS2-type substitu-

tion.⁸ Additional GG-selective photocleavage agents have been reported by others.^{25–28}

In the mechanism of these cleavage reactions, after intercalation and photoexcitation, an electron is transferred to the excited state of an intercalated AQS2 molecule from a flanking DNA base, to generate a radical cation on the base. The three-dimensional structure of the DNA complex and molecular orbital calculations described here confirm that such electron transfer is enabled by intimate van der Waals contact and molecular orbital overlap of AQS2 with DNA bases.

We have shown previously that the radical cation formed upon electron transfer to an intercalated chromophore migrates from the base adjacent to the intercalated AQS2 to a GG step where it is trapped by reaction with water and/or molecular oxygen. This model of radical cation migration to remote sites followed by covalent damage is supported by observations of GG cleavage by rhodium complexes or AQ derivatives that are covalently linked to DNA. Even when located over 10 base pairs from a confined photocleavage agent, GG sites are cleaved selectively.^{15,28}

The radical cation migration model is consistent with calculations suggesting that GG steps are the most easily oxidized of all B-conformation dinucleotides.²⁹ In ideal B-conformation, the electron rich N⁷ atom of guanine on the 3' side of the GG step is positioned over the centroid of the five-membered ring of the 5'-G. The 3'-guanine would thus stabilize a radical cation on the 5'-guanine.³⁰ However, product ratios are determined by differences in energies of transition states.³¹ The 5'- or 3'-localized guanine radical cations in a GG step are reactive intermediates, not transition states. The energies of these intermediates do not necessarily predict 5' or 3' reaction product ratios.

Three-Dimensional Structure of an AQS2–DNA Complex. AQS2 forms an unusual groove-reversed complex, with the swallow tail located in the major groove (Figures 5 and 6). Generally intercalators interact preferentially with the minor groove. Daunomycin (Figures 1, 5, and 6) and nearly all intercalators bind to DNA with out-of-plane substituents located in the minor groove.^{32–37} The minor groove of B-DNA forms a natural cleft, affording more favorable van der Waals interactions than the major groove. In com-

(25) Saito, I.; Takayama, M.; Kawanishi, S. *J. Am. Chem. Soc.* **1995**, *117*, 5590–5591.

(26) Saito, I.; Takayama, M.; Sugiyama, H.; Nakatani, K.; Tsuchida, A.; Yamamoto, M. *J. Am. Chem. Soc.* **1995**, *117*, 6406–6407.

(27) Ito, K.; Inoue, S.; Yamamoto, K.; Kawanishi, S. *J. Biol. Chem.* **1993**, *268*, 13221–13227.

(28) Hall, D. B.; Holmlin, R. E.; Barton, J. K. *Nature* **1996**, *382*, 731–735.

(29) Sugiyama, H.; Saito, I. *J. Am. Chem. Soc.* **1996**, *118*, 7063–7068.

(30) Prat, F.; Houk, K. N.; Foote, C. S. *J. Am. Chem. Soc.* **1998**, *120*, 845–846.

(31) Hammett, L. P. *Physical Organic Chemistry Reaction Rates, Equilibria and Mechanisms*; McGraw-Hill: New York, 1979.

(32) Wang, A. H.; Ughetto, G.; Quigley, G. J.; Rich, A. *Biochemistry* **1987**, *26*, 1152–63.

(33) Williams, L. D.; Egli, M.; Ughetto, G.; van der Marel, G. A.; van Boom, J. H.; Quigley, G. J.; Wang, A. H.-J.; Rich, A.; Frederick, C. A. *J. Mol. Biol.* **1990**, *215*, 313–320.

(34) Hu, G. G.; Shui, X.; Leng, F.; Priebe, W.; Chaires, J. B.; Williams, L. D. *Biochemistry* **1997**, *36*, 5940–5946.

(35) Frederick, C. A.; Williams, L. D.; Ughetto, G.; van der Marel, G. A.; van Boom, J. H.; Rich, A.; Wang, A. H.-J. *Biochemistry* **1990**, *29*, 2538–2549.

(36) Williams, L. D.; Egli, M.; Gao, Q.; Bash, P.; van der Marel, G. A.; van Boom, J. H.; Rich, A.; Frederick, C. A. *Proc. Natl. Acad. Sci. U.S.A.* **1990**, *87*, 2225–2229.

(37) Williams, L. D.; Frederick, C. A.; Ughetto, G.; Rich, A. *Nucleic Acids Res.* **1990**, *18*, 5533–5541.

parison with daunomycin, the switch to the major groove results from a rotation of AQS2 by 105° around the DNA helical axis.

We have considered several possible origins for groove-reversal of intercalated complexes. Specific, orientation-dependent interactions between intercalated ring systems and flanking base pairs might favor groove-reversal.³⁸ Intercalator–base interactions could offset the lack of minor groove interactions. The importance of specific intercalator–base interactions in groove-reversed complexes is supported by the base selectivity of the van der Waals interactions (stacking) observed in each groove-reversed complex solved thus far by X-ray diffraction. Preferential stacking of guanines is observed in the AQS2 complex here and in a bis-intercalated DNA–ditercalinium complex.³⁸ Ditercalinium forms 68 contacts with guanine residues and only 5 with cytosine residues.³⁸ Preferential stacking of intercalators on guanine bases is not a general feature of intercalated complexes and is not observed in minor groove intercalated complexes. Daunomycin stacks nonselectively in X-ray structures of daunomycin–DNA complexes.³² Each of the four bases that flank daunomycin engages in nearly the same number of contacts with planar surfaces of daunomycin [cytosine (1), 7 contacts; guanine (2), 8 contacts; cytosine (11), 7 contacts; guanine (12), 7 contacts]. This lack of preference of daunomycin for guanines is apparent in the axial views of Figure 6C,D.

The structure of the AQS2–DNA complex suggests that groove-reversal might also be favored by polyamine-like interactions within the major groove. Polyamines bind preferentially in the major groove of B-DNA in dynamic and disordered complexes.^{39,40} The swallow tail of AQS2 is similar to a polyamine, with cationic amino groups separated by a flexible and hydrophobic hydrocarbon linker. Thus competing hydrophobic, charge–charge and hydrogen-bonding interactions that direct spermine to the major groove may similarly direct the swallow tail of AQS2 to the major groove. In the present structure, lattice interactions might also favor groove reversal. The swallow tail makes several hydrogen bonds to adjacent duplexes in the crystal lattice.

Differences in binding mode of AQS2 (groove-reversed intercalation) and daunomycin (minor groove intercalation) do not appear to arise from differences in molecular shapes. The shape of AQS2 is similar to that of daunomycin. Each of these intercalators is composed of an elongated planar chromophore joined with out-of-plane substituents along the long axis of the chromophore. The amino sugar of daunomycin and the swallow tail of AQS2 are positively charged (+2 AQS2, +1 daunomycin).

The similar shapes of the two intercalators appear to induce similar DNA distortion. The conformation of the DNA in the AQS2–d(CGTAACG) complex described here shows similarities to that of the daunomycin–d(CGTAACG) complex.³² Helical parameters for the AQS2 complex and differences in helical parameters of AQS2 and daunomycin complexes (Table 2) show that in both structures (i) the DNA is unwound by only a few degrees at the intercalation site and (ii) base pair G(2)–C(11) is buckled by over 15°, wrapping around the intercalator to maximize van der Waals contacts.²⁴

Observed differences in binding modes of the two intercalators (minor groove intercalation versus groove-reversed

intercalation) cause differences in the DNA conformations of the AQS2–d(CGTAACG) complex and daunomycin–d(CGTAACG) complex. The winding angle at the intercalation site is less in the AQS2 complex than in the daunomycin complex. This observation is consistent with our previous hypothesis²⁴ that low helical twist (DNA unwinding) at the intercalation step is a characteristic of parallel intercalator orientation. The long axis of AQS2 is aligned roughly parallel with the long axis of the flanking base pairs (Figure 6A,B) whereas the long axis of daunomycin is aligned roughly perpendicular with the long axis of the flanking base pairs (Figure 6C,D). Therefore, the greater unwinding at the intercalation step by AQS2 than by daunomycin (Table 2) is consistent with our hypothesis.

Base pair C(1)–G(12) is significantly less buckled in the AQS2 complex (–0.8°) than in the daunomycin complex (–9.1°). This difference is directly attributable to differences in the orientations of the chromophores relative to that base pair. In the parallel orientation of the AQS2 complex, the base pair is flattened by the chromophore; van der Waals interactions are maximized by maintaining planarity of the base pair.²⁴ In the perpendicular orientation of the daunomycin complex (Figure 6C), van der Waals contacts with the chromophore are maximized by deforming (buckling) the adjacent base pair.²⁴

Conclusion

Intercalation of anthraquinone photonucleases is necessary for efficient photocleavage of DNA at GG steps.⁸ The X-ray structure of the AQS2 complex confirms this requirement for intercalation and can help to rationalize several steps in the photocleavage reaction. The reaction can be conceptually broken down into distinct and sequential steps: intercalation, photoexcitation, base to AQS2 electron transfer, base to base hole migration, trapping, and covalent oxidative damage. This X-ray structure is relevant to intercalation, photoexcitation, electron transfer, and hole migration but not to trapping and covalent oxidative damage. The structure does not contain GG steps and so cannot explain terminal steps in the reaction. The three-dimensional structure of a complex containing a GG step would be relevant to hole migration, trapping, and covalent oxidative damage, but thus far we have not obtained diffraction-quality crystals of such a complex.

The 3-D structure of the complex allows us to understand several critical aspects of the reaction mechanism.

(i) Base to AQS2 Electron Transfer. The requirement for intercalation suggests that extensive anthraquinone–base interactions are necessary for rapid electron transfer. Selective van der Waals interaction of ground state AQS2 with guanine residues and significant molecular orbital overlap within the intercalated complex would pose the complex for efficient electron transfer after photoexcitation. Guanine, the most easily oxidized DNA base, provides the most thermodynamically accessible source of electrons.

(ii) Hole Migration. The bases adjacent to the intercalation site and in the interior of the complex are well-stacked. It is likely that hole migration within DNA requires significant electronic overlap of adjacent DNA bases.

This requirement for electronic overlap is supported by the structure and reactivity of DNA–porphyrin complexes. Brun and Harriman⁴¹ previously described inefficient electron exchange between palladium porphyrins bound to DNA. The

(38) Williams, L. D.; Gao, Q. *Biochemistry* **1992**, *31*, 4315–4324.

(39) Wemmer, D. E.; Srivenugopal, K. S.; Reid, B. R.; Morris, D. R. *J. Mol. Biol.* **1985**, *185*, 457–459.

(40) Shui, X.; McFail-Isom, L.; Hu, G. G.; Williams, L. D. *Biochemistry* **1998**, *37*, 8341–8355.

(41) Brun, A. M.; Harriman, A. *J. Am. Chem. Soc.* **1994**, *116*, 10383–10393.

X-ray structure of a DNA–porphyrin complex⁴² reveals poor van der Waals contacts within that complex.

In sum, it appears that intimate contacts are necessary for electron transfer from base to intercalator and from base to base within DNA.

(42) Lipscomb, L. A.; Zhou, F. X.; Presnell, S. R.; Woo, R. J.; Peek, M. E.; Plaskon, R. R.; Williams, L. D. *Biochemistry* **1996**, *35*, 2818–2823.

Acknowledgment. This work was funded by the National Science Foundation (Grant MCB-9056300, to L.D.W.), the American Cancer Society (Grant RPG-95-116-03-GMC, to L.D.W.), and the National Institutes of Health (Grant GM28190, to G.B.S.).

JA981761T